Journal of Power Sources 196 (2011) 182–185

Contents lists available at ScienceDirect

Journal of Power Sources

journal homepage: www.elsevier.com/locate/jpowsour

Short communication

Carbon nanotubes supported Fe-based compounds as the electrode catalyst for oxygen reduction reaction

Kun Ning Zhu[a], Hai Ying Qin[a], Bin Hong Liu[b], Zhou Peng Li[a,*]

[a] Department of Chemical and Biological Engineering, Zhejiang University, Zeda Road 38, Hangzhou 310027, Zhejiang, PR China
[b] Department of Materials Science and Engineering, Zhejiang University, Hangzhou 310027, PR China

ARTICLE INFO

Article history:
Received 23 April 2010
Received in revised form 14 June 2010
Accepted 15 June 2010
Available online 23 June 2010

Keywords:
Amorphous catalyst
Iron-based electrocatalyst
Oxygen reduction reaction
Electrocatalytic activity
Cell performance

ABSTRACT

An amorphous Fe-based catalyst supported on polypyrrole-modified carbon nanotubes is synthesized by a chemical method. The microstructure, surface composition and morphology are characterized by X-ray diffraction, X-ray photoelectron spectroscopy, and scanning electron microscopy. The synthesized amorphous Fe-based catalyst is composed of amorphous FeOOH and microcrystalline Fe_2O_3. Compared with a crystalline FeOOH catalyst, the amorphous Fe-based catalyst demonstrates higher electrocatalytic activity toward the oxygen reduction reaction (ORR), due to its amorphous structure and large specific surface area. It is considered that amorphization of transition metal compounds could be one of the methods used to improve their catalytic activity toward the ORR.

1. Introduction

Proton exchange membrane fuel cells (PEMFCs) have been recognized as the clean power generators with high efficiency for mobile and portable applications due to their high power densities and low emissions. PEMFCs use Pt as the catalyst where the hydrogen oxidation reaction (HOR) or the oxygen reduction reaction (ORR) occurs. However, the scarcity of Pt in nature is a big problem for PEMFC commercialization. Therefore, development of alternative materials to Pt is one of the critical issues because cell performance is mainly determined by kinetics of the ORR.

Non-precious metals such as Cu [1], Ni [2], Ag [3,4] and Co [5–7], inorganic compounds such as TiO_2 [8], vanadium oxides [9], lanthanum manganite [10], MnO_2 [11–13], iron nitrides [14], Co nitrides [15] and Co hydroxide [16–18] were attempted to be used as the cathode catalysts in fuel cells. Macrocyclic compounds such as metallic porphyrins [19], phthalocyanines [20] and their modified catalysts [5–7,16–18,21] demonstrated good electrocatalytic activities toward the ORR. Ramos-Sánchez et al. [22] studied the electrocatalytic activity of amorphous $Ni_{59}Nb_{40}Pt_xM_{1-x}$ (M = Ru, Sn) toward the ORR. It was found that the amorphous catalysts showed the high activity toward the ORR via a 4e transfer pathway. Incorporation of transition metals in amorphous catalysts demonstrated a significant improvement on the ORR kinetics. Yang and Xu [23] investigated the electrocatalytic activity of an amorphous manganese oxide for the ORR in alkaline solutions. They believed that amorphous materials owned much more structure distortion and thus yielded more active sites than crystalline ones. Recent progress in the development of alternative catalysts has been summarized [24,25]. However, only few studies are related to amorphous catalysts.

It is considered that Fe^{3+} ions could be chemically reduced to form $Fe(OH)_2$ in alkaline borohydride solutions by following reaction:

$$4Fe^{3+} + BH_4^- + 12OH^- = 4Fe(OH)_2\downarrow + BO_2^- + 2H_2O + 2H_2\uparrow \quad (1)$$

The formed ultrafine particles of $Fe(OH)_2$ would then be oxidized to ultrafine FeOOH crystal in air by following reaction [26,27]:

$$4Fe(OH)_2 + O_2 = 4FeOOH + 2H_2O \quad (2)$$

In this work, amorphous FeOOH and crystalline FeOOH supported on polypyrrole-modified carbon nanotubes are synthesized and characterized to study the effect of the amorphous structure on the improvement of the electrocatalytic activity toward the ORR. Their electrocatalytic activities are evaluated by cyclic voltammetry (CV) and cell polarization in an alkaline fuel cell using an alkaline borohydride solution as the fuel.

* Corresponding author. Tel.: +86 571 87951977; fax: +86 571 87953149.
E-mail address: zhoupengli@zju.edu.cn (Z.P. Li).

0378-7753/$ – see front matter © 2010 Elsevier B.V. All rights reserved.
doi:10.1016/j.jpowsour.2010.06.046

Table 1
Relative atomic ratio of constituents in the surface layer of the synthesized catalysts.

	C	O	N	Fe
Catalyst A (crystalline FeOOH catalyst)	58.0%	27.5%	6.4%	8.2%
Catalyst B (amorphous FeOOH catalyst)	59.2%	26.3%	6.6%	7.8%

2. Experimental

2.1. Catalyst synthesis

Carbon nanotubes supported Fe-based catalysts were prepared by following steps:

(1) mixing carbon nanotubes (CNTs) (1.1 g) with glacial acetic acid (2 mL) and de-ionized water (100 mL) in a round-bottom flask placed in an ice-water bath by stirring for 5 min;
(2) adding 0.6 mL of pyrrole, and then stirring for 20 min before adding a $FeCl_3$ solution containing 0.869 g of $FeCl_3$ and 50 mL of de-ionized water;
(3) stirring for 20 min in a dark environment, and then slowly adding H_2O_2 solution (22 mL, 3 wt.% H_2O_2) during stirring for 90 min;
(4) adding an alkaline solution (50 mL containing 3.8 wt.% NaOH,) or alkaline borohydride solution (52 mL, 3.8 wt.% $NaBH_4$, 3.8 wt.% NaOH), and stirring for 30 min.

Finally, the mixture was filtered, washed by de-ionized water, and dried overnight at 90 °C to obtain the Fe-based compounds supported on polypyrrole-modified carbon nanotubes. The catalysts synthesized by adding alkaline solutions with and without borohydride addition were named as "catalyst A" and "catalyst B", respectively. Fe content in both samples was about 15 wt.% which was confirmed by induced coupled plasma spectrum (ICP) measurements.

2.2. Catalyst characterization

The microstructure and morphology of polypyrrole-modified carbon nanotubes supported Fe-based catalysts were characterized by X-ray diffraction (XRD) with a Rigaku-D/MAX-2550PC diffractometer using Cu K_α radiation (λ = 1.5406 Å), and scanning electron microscopy (SEM). X-ray photoelectron spectroscopy (XPS) analyses using Mg K_α radiation with a PHI-5000C ESCA system were carried out to identify the surface composition and the chemical state of Fe and O.

2.3. Electrochemical evaluation

The electrocatalytic activity toward the ORR was evaluated by CV technique in a KOH solution (1 M) saturated with O_2. A catalyst ink was prepared by ultrasonically mixing 10 mg of catalyst with 100 μL of Nafion solution (5 wt.%) and 500 μL of anhydrous ethanol for 30 min. The obtained ink (10 μL) was then dropped onto a glassy carbon electrode (0.07 cm^2). A porous catalyst layer was formed on a glassy carbon electrode after drying at room temperature in air. CV measurements were performed in a three-electrode system with a scan rate of 10 mV s^{-1} at 25 °C. A Pt wire was used as the counter electrode, and a saturated calomel electrode was used as the reference electrode connecting to a three-electrode cell with a KCl salt bridge. Potential values were converted to the values vs. standard hydrogen electrode (SHE).

Cell performances were measured by using a fuel cell as described in our previous paper [16]. A cathode was prepared by coating cathode ink onto a piece of hydrophobic carbon cloth with a catalyst loading of 5 mg cm^{-2}. A cathode ink was prepared by mixing catalyst, de-ionized water, Nafion solution (5 wt.%), and anhydrous ethanol with a mass ratio of 1:3:7:3. The hydrophobic carbon cloth was prepared by immersing the cloth in polytetrafluoroethylene (PTFE) emulsion (20 wt.%) for 3 min and then heating at 350 °C for 1 h. A Co-PPy/C composite was used as the anode catalyst as described in our previous work [7]. An anode was prepared by pasting an anode ink onto a piece of nickel foam with a catalyst loading of 5 mg cm^{-2}.

An alkaline $NaBH_4$ solution containing 5 wt.% of $NaBH_4$ and 10 wt.% of NaOH was used as the fuel. Cell performance measurement was carried out at a fuel flow rate of 10 mL min^{-1} and a humidified O_2 flow rate of 150 mL min^{-1}. Temperature of both fuel and humidified O_2 was controlled to be 80 °C.

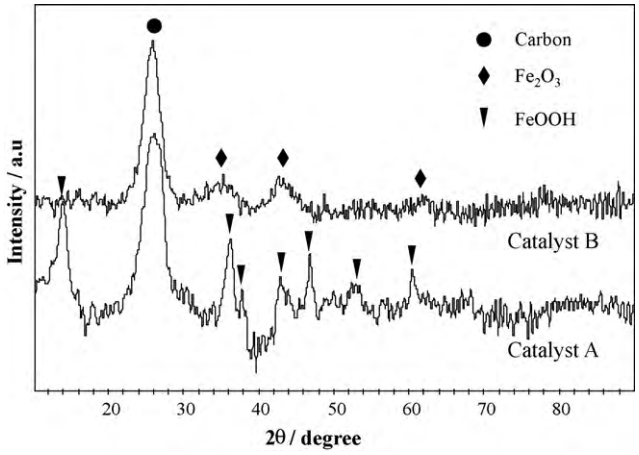

Fig. 1. XRD patterns of catalyst A (crystalline FeOOH catalyst) and catalyst B (amorphous FeOOH catalyst).

3. Results and discussion

3.1. Catalyst characterization

Fig. 1 shows the XRD patterns of catalyst A and B. The strong peak at 26.34° in 2θ can be assigned to the (1 1 1) plane of carbon (JCPDS number: 75-0444). The XRD pattern of catalyst A reveals the FeOOH existence regarding to JCPDS number 70-0714. However, no crystalline FeOOH except carbon and small amount of microcrystalline Fe_2O_3 is confirmed from the XRD pattern of catalyst B. Because both samples contain the same amount of Fe according to the ICP results, the XRD result implies that some amorphous iron compounds might be formed in catalyst B.

Fig. 2 gives the XPS results of the binding energies of Fe 2p and O 1s electrons in the synthesized catalysts. It can be seen that the binding energies of Fe 2p electrons of catalyst A demonstrate a typical pattern of FeOOH [28], which agrees with the XRD result. The corresponding Fe 2p peak areas of catalyst A and B as shown in Fig. 2(a), reveal that they have equivalent amount of iron. The relative atomic ratio of each constituent in the surface layer is illustrated in Table 1. Carbon is from CNTs and polypyrrole (PPy). Nitrogen is from PPy. According to the atomic ratio of Fe in the surface layer, the Fe contents in the surface layer of catalyst A and catalyst B are calculated to be 27.2 wt.% and 26.3 wt.%, respectively, which are larger than those obtained by ICP measurements. The difference between the XPS and ICP measurements can be attributed to the fact that XPS gives the catalyst surface composition while the ICP analysis includes the catalyst support.

The binding energies of O 1s electrons of the catalysts reveal that the binding situations of OH^- and O^{2-} with Fe in catalyst B are similar to that in catalyst A as shown in Fig. 2(b). Calculated from the XPS peak area of O 1s, the oxygen content on the surface of catalyst

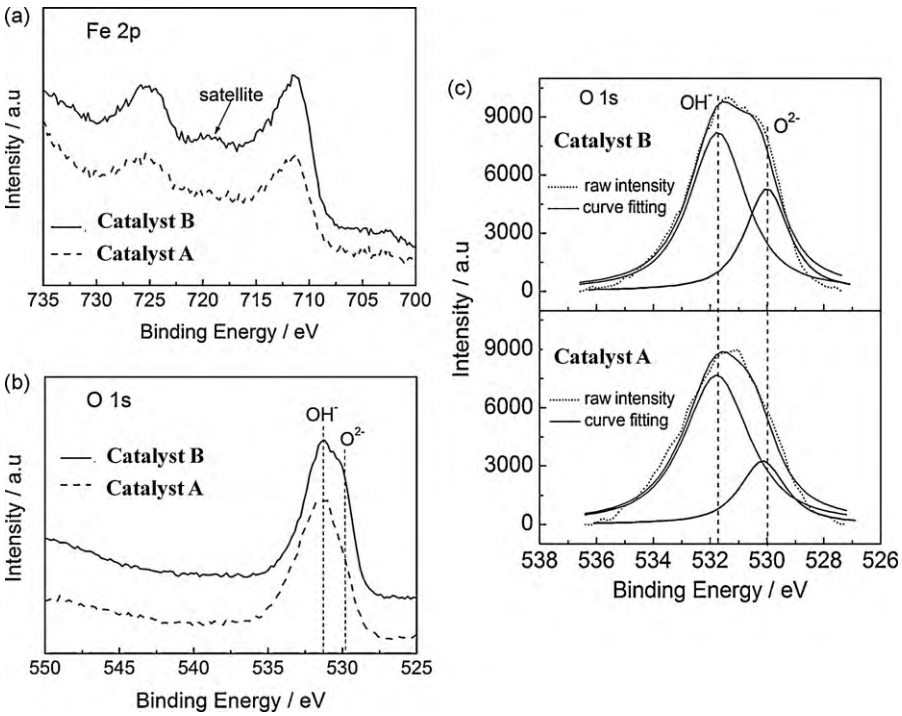

Fig. 2. Binding energies of Fe 2p electrons (a) and O 1s electrons (b) in synthesized catalysts, curve fitting of O 1s with Shirley background subtraction (c).

B (Fe/O = 1/3.37) is equivalent to that of catalyst A (Fe/O = 1/3.35) as shown in Table 1. In order to identify the portions of OH^- and O^{2-} in the surface layer of the catalysts, curve fitting of the binding energy of O 1s electron was conducted as shown in Fig. 2(c). It is clear that both catalysts contain the same content of OH^-. From these results, it can be concluded that catalyst B is composed of amorphous FeOOH. Here for convenience, catalyst A and catalyst B are nominated as crystalline FeOOH catalyst and amorphous FeOOH catalyst, respectively.

As shown in Fig. 2(a), the presence of Fe $2p_{3/2}$ satellite peak located at 719 eV indicates the existence of Fe_2O_3 in amorphous FeOOH catalyst as satellite peak at 719 eV is the characteristic peak of Fe_2O_3 [29]. O 1s electrons of the amorphous FeOOH catalyst and the crystalline FeOOH catalyst exist in two chemical states with binding energy of 529.6 eV and 531.7 eV, respectively. It is known that O 1s peaks located at 529.6 eV and 531.7 eV can be referred to O 1s electron emissions from O^{2-} and OH^-, respectively [28,30]. The higher content of O^{2-} in the amorphous FeOOH catalyst can be attributed to the fact that no OH^- but only O^{2-} exists in Fe_2O_3. Therefore, it can be concluded that the amorphous FeOOH catalyst is composed of amorphous FeOOH and microcrystalline Fe_2O_3.

Because of the magnetism of Fe-based catalysts, it is technically difficult to perform TEM (transmission electron microscopy) observations. Fig. 3 gives SEM images of the synthesized catalysts. It can be seen that either amorphous or crystalline FeOOH has been loaded on carbon nanotubes. The crystalline FeOOH is larger than the amorphous FeOOH in size.

3.2. Electrochemical evaluation

Fig. 4 presents cyclic voltammograms of the glassy carbon (GC) electrodes modified by the CNTs supported crystalline FeOOH catalyst and the CNTs supported amorphous FeOOH catalyst in 1 M KOH solution saturated with argon or oxygen at 25 °C with a scan rate of 10 mV s^{-1}. In the 1 M KOH solution saturated with oxygen, the electrode using amorphous FeOOH catalyst exhibits a larger reduction current than that using the crystalline FeOOH catalyst as shown in Fig. 4(b). Fig. 5 gives a cell performance comparison of corresponding testing cells using amorphous and crystalline FeOOH as the cathode catalyst. It can be seen that the cell using the amorphous FeOOH catalyst exhibits lower polarization and higher performance than that using the crystalline FeOOH catalyst. According to the results as shown above, it can be concluded that the amorphous FeOOH catalyst has higher electrocatalytic activity toward the ORR than the crystalline FeOOH catalyst. It is considered that the amorphous structure may play an important role in the cell performance improvement, as Ramos-Sánchez suggested [22].

In the alkaline solution saturated with argon, a typical charge and discharge loop of a capacitor is demonstrated whether the GC electrode is modified by the CNTs supported crystalline FeOOH

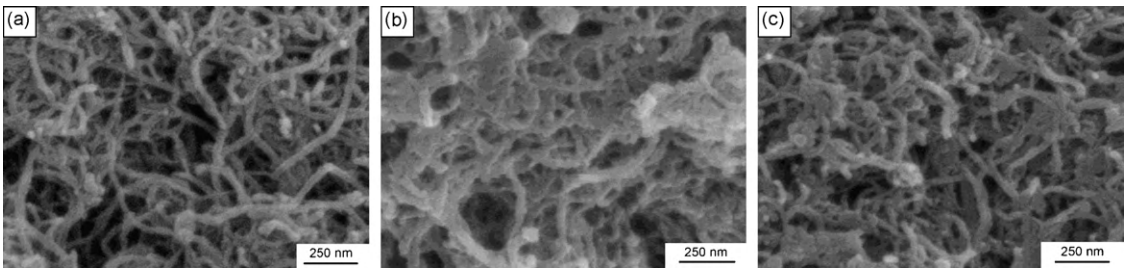

Fig. 3. SEM images of CNTs (a), crystalline FeOOH catalyst (b), and amorphous FeOOH catalyst (c).

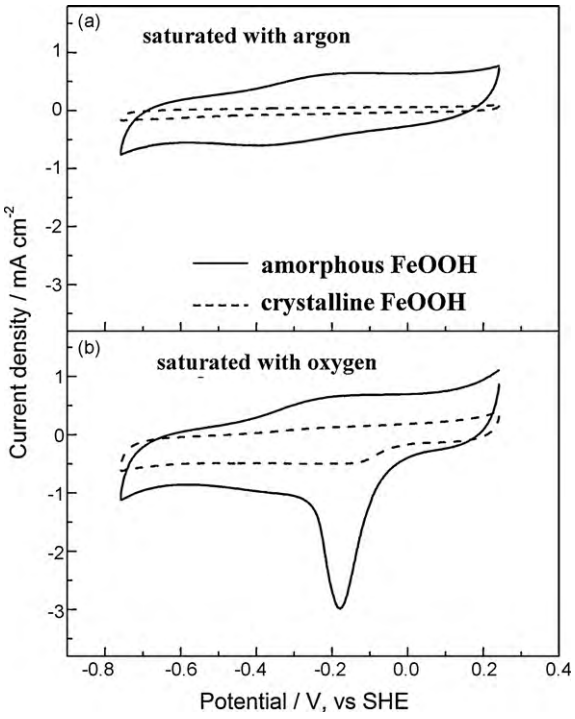

Fig. 4. CV curves of amorphous FeOOH catalyst and crystalline FeOOH catalyst in 1 M KOH solution saturated with argon (a) or oxygen (b) with a scan rate of 10 mV s^{-1} at 25 °C.

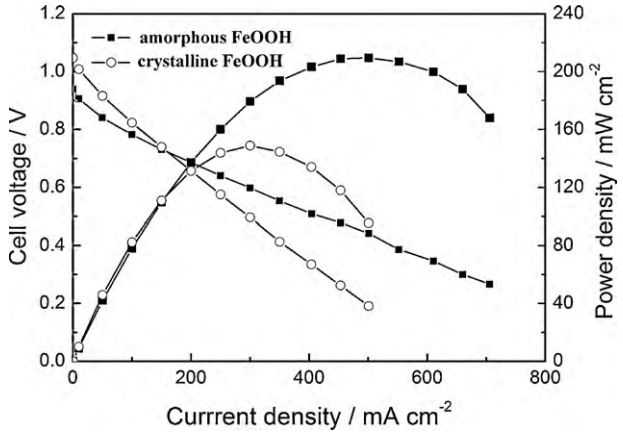

Fig. 5. Performance comparison of the cell using amorphous FeOOH catalyst with that using crystalline FeOOH catalyst as the cathode catalyst in the direct borohydride fuel cell.

catalyst or by the CNTs supported amorphous FeOOH catalyst as shown in Fig. 4(a). It can be seen that the GC electrode modified by the amorphous FeOOH catalyst exhibits higher charge and discharge currents comparing with that modified by the crystalline FeOOH catalyst. This result reveals that the electrode modified by the amorphous FeOOH catalyst has larger capacitance than that modified by the crystalline FeOOH catalyst. This result implies that the specific surface area of the amorphous FeOOH catalyst is larger than that of the crystalline FeOOH catalyst because capacitance is proportional to specific surface area in a porous electrode. This deduction agrees with the SEM observation. Therefore, the large specific surface area is another factor to improve the electrocatalytic activity of the amorphous FeOOH catalyst.

4. Conclusions

An amorphous Fe-based catalyst supported on polypyrrole-modified CNTs is synthesized by a chemical method. The synthesized amorphous catalyst is composed of amorphous FeOOH and microcrystalline Fe_2O_3, exhibiting higher electrocatalytic activity toward the ORR than the crystalline FeOOH catalyst. The good electrocatalytic activity of the amorphous FeOOH catalyst can be attributed to its amorphous structure and large specific surface area.

Acknowledgements

This work is financially supported by Hi-tech Research and Development Program of China (863), grant no. 2007AA05Z144; Doctoral fund from Education ministry of China (20070335003); China Postdoctoral Science Foundation (20090461364); and the National Natural Science Foundation of China, grant nos. 20976156 and 50971114.

References

[1] S. Ohno, K. Yagyuu, K. Nakatsuji, F. Komori, Surf. Sci. 554 (2004) 183–192.
[2] B. Lescop, J.Ph. Jay, G. Fanjoux, Surf. Sci. 548 (2004) 83–94.
[3] H. Cheng, K. Scott, K. Lovell, Fuel Cells 6 (2006) 367–375.
[4] B.H. Liu, S. Suda, J. Power Sources 164 (2007) 100–104.
[5] R. Bashyam, P. Zelenay, Nature 443 (2006) 63–66.
[6] K. Asazawa, K. Yamada, H. Tanaka, A. Oka, M. Taniguchi, T. Kobayashi, Angew. Chem. Int. Ed. 46 (2007) 8024–8027.
[7] H.Y. Qin, Z.X. Liu, W.X. Yin, J.K. Zhu, Z.P. Li, J. Power Sources 185 (2008) 909–912.
[8] S.V. Mentus, Electrochim. Acta 50 (2004) 27–32.
[9] B.R. Limoges, R.J. Stanis, J.A. Turner, A.M. Herring, Electrochim. Acta 50 (2005) 1169–1179.
[10] M. Hayashi, H. Uemura, K. Shimanoe, N. Miura, N. Yamazoe, J. Electrochem. Soc. 151 (2004) A158–A163.
[11] R.X. Feng, H. Dong, Y.D. Yang, X.P. Ai, Y.L. Cao, H.X. Yang, Electrochem. Commun. 7 (2005) 449–452.
[12] Y.G. Wang, Y.Y. Xia, Electrochem. Commun. 8 (2006) 1775–1778.
[13] M. Chatenet, F. Micoud, I. Roche, E. Chainet, J. Vondrák, Electrochim. Acta 51 (2006) 5452–5458.
[14] C. Medard, M. Lefevre, J.P. Dodelet, F. Jaouen, G. Lindbergh, Electrochim. Acta 51 (2006) 3202–3213.
[15] A.L. Bouwkamp-Wijnoltz, W. Visscher, J.A.R. van Veen, S.C. Tang, Electrochim. Acta 45 (1999) 379–386.
[16] H.Y. Qin, Z.X. Liu, L.Q. Ye, J.K. Zhu, Z.P. Li, J. Power Sources 192 (2009) 385–390.
[17] H.Y. Qin, Z.X. Liu, S.J. Lao, J.K. Zhu, Z.P. Li, J. Power Sources 195 (2010) 3124–3129.
[18] H.Y. Qin, S.J. Lao, Z.X. Liu, J.K. Zhu, Z.P. Li, Int. J. Hydrogen Energy 35 (2010) 1872–1878.
[19] H. Cheng, K. Scott, J. Electroanal. Chem. 596 (2006) 117–123.
[20] J.F. Ma, Y.N. Liu, P. Zhang, J. Wang, Electrochem. Commun. 10 (2008) 100–102.
[21] S. Maldonado, K.J. Stevenson, J. Phys. Chem. B 108 (2004) 11375–11383.
[22] G. Ramos-Sánchez, A.R. Pierna, O. Solorza-Feria, J. Non-Cryst. Solids 354 (2008) 5165–5168.
[23] J. Yang, J.J. Xu, Electrochem. Commun. 5 (2003) 306–311.
[24] B. Wang, J. Power Sources 152 (2005) 1–15.
[25] Z.P. Li, B.H. Liu, J. Appl. Electrochem. 40 (2010) 475–483.
[26] X. Liu, G. Qiu, A. Yan, Z. Wang, X. Li, J. Alloy Compd. 433 (2007) 216–220.
[27] S. Krehula, S. Music, J. Alloy Compd. 416 (2006) 284–290.
[28] Q. Gao, F.H. Chen, J.L. Zhang, G.Y. Hong, J.Z. Ni, X. Wei, D.J. Wang, J. Magn. Magn. Mater. 321 (2009) 1052–1057.
[29] H. Liu, E.Y. Jiang, R.K. Zheng, H.L. Bai, Phys. Stat. Solidi A 201 (2004) 739–744.
[30] H. Abdel-Samad, P.R. Watson, Appl. Surf. Sci. 136 (1998) 46–54.